Systematic investigation and in vitro biocompatibility studies on mesoporous europium doped hydroxyapatite

Cristina L. Popa, Carmen Steluta Ciobanu, Simona Liliana Iconaru, Miruna Stan, Anca Dinischiotu, Constantin C. Negrila, Mikael Motelica-Heino, Régis Guégan, Daniela Predoi

Systematic investigation and *in vitro* biocompatibility studies on mesoporous europium doped hydroxyapatite

Cristina Liana Popa
National Institute of Materials Physics, Atomistilor Str., No. 105 bis PO Box MG 7, 077125, Magurele, Romania.

Carmen Steluta Ciobanu,
National Institute of Materials Physics, Atomistilor Str., No. 105 bis PO Box MG 7, 077125, Magurele, Romania.

Simona Liliana Iconaru
National Institute of Materials Physics, Atomistilor Str., No. 105 bis PO Box MG 7, 077125, Magurele, Romania.
Institute for Eath Sciences, UMR 7327, CNRS-University of Orléans, 1A Rue de la Férrolerie, 45071 Orléans cedex 02, France

Miruna Stan,
Department of Biochemistry and Molecular Biology, University of Bucharest, 91-95 Spl. Independentei, 050095, Bucharest, Sector 5, Romania

Anca Dinischiotu,
Department of Biochemistry and Molecular Biology, University of Bucharest, 91-95 Spl. Independentei, 050095, Bucharest, Sector 5, Romania

Constantin Catalin Negrila,
National Institute of Materials Physics, Atomistilor Str., No. 105 bis PO Box MG 7, 077125, Magurele, Romania.

Mikael Motelica-Heino,
Institute for Earth Sciences, UMR 7327, CNRS-University of Orléans, 1A Rue de la Férrolerie, 45071 Orléans cedex 02, France

Regis Guegan,
Institute for Earth Sciences, UMR 7327, CNRS-University of Orléans, 1A Rue de la Férrolerie, 45071 Orléans cedex 02, France

Daniela Predoi
National Institute of Materials Physics, Atomistilor Str., No. 105 bis PO Box MG 7, 077125, Magurele, Romania. [*]dpredoi@gmail.com

Abstract

This paper reports a systematic investigation on europium doped hydroxyapatite (Eu:HAp). In this work, a set of complementary techniques Fourier Transform Infrared spectroscopy (FTIR), X-ray photoelectron spectroscopy (XPS), transmission electron microscopy (TEM) and, Brunauer–Emmett–Teller (BET) technique was used to allowing a proper understanding of Eu:HAp. The XPS analysis confirmed the substitution of Ca ions by Eu ions in Eu:HAp samples. Eu:HAp and pure HAp show the isotherms of type IV with a hysteresis loop at a relative pressure (P/P_0) between 0.4 and 1.0, indicating the presence of mesopores. Finally, the *in vitro* biological effects of Eu:HAp nanoparticles were evaluated by focusing on F-actin filaments pattern and heat shock proteins (Hsp) expression in HEK293 human kidney cells. Fluorescence microscopy studies of the actin protein revealed no changes of the immunolabeling profile in the renal cells cultured in the presence of Eu:HAp nanoparticles. Hsp60, Hsp70 and Hsp90 expression measured by Western blot analysis were not affected after a 24 and 48 hours exposure. These results confirmed the lack of nanoparticles' toxicity and the biocompatibility of Eu:HAp nanoparticles and their possibility possible uses of using them in medical purposes without affecting the renal function.

Keywords: nanoparticles, hydroxyapatite, europium, *in vitro* studies

1. Introduction

Hydroxyapatite (HAp) is one of the most studied inorganic materials due to its excellent biological properties. Belonging to the apatite family, HAp, with the general formula, $Ca_{10}(PO_4)_6(OH)_2$ constitutes the most important inorganic component of bones and teeth of about 65% of the total mineral content of the human bone mineral component, being the most important inorganic component of bones and teeth [1-5]. Moreover, synthetic HAp has given promising results in the area of drug storage and damaged bone reconstruction. Intensive studies have shown an incredible biocompatibility, osteoconductivity, non-toxic and non-inflammatory properties. HAp nanostructures are suitable for both bio-imaging and drug delivery. Among the several routes for the synthesis of HAp, the co-precipitation method has attracted great attention with its ability to generate nanoscale particles and nanocrystalline powders at low processing temperature. By co-precipitation method both size and morphology of the synthesized nanoparticles can be controlled which is of fundamental importance in the process of calcium phosphate deposition to the formation of renal stones [6].

One of the most important properties of hydroxyapatite is the ability to incorporate a wide variety of substitutions for Ca^{2+}, PO_4^{3-} and/or OH^- ions based on the flexibility of the apatite structure. Trivalent europium Eu ions have been used as luminescent probes in the investigation of crystallographic structure of activator centres, as well as a tool to probe the local symmetry and occupancy of cationic sites in apatite structures. A. Doat et al. showed that Eu^{3+} ion luminescence can be obtained under visible irradiation [7]. Eu^{3+} ion luminescence obtained by visible irradiation is suitable for prolonged examination of living cells. Different synthesis techniques for the study of the substitution of Ca^{2+} by Eu^{3+} ions have been reported in previous research. R.S. André et al. [8] obtained, by using a microwave hydrothermal method, Eu-doped hydroxyapatite (Eu:HAp) nanorod with diameters from 9 to 26 nm. Eu^{3+} ions were used as a

marker in the HAp network by basic hydrolysis followed by the microwave hydrothermal method synthesis treatment process. C.A. Barta et al. reported that Eu^{3+} ions have the potential for the treatment of bone density disorders such as osteoporosis [9]. However, the as-prepared $Eu^{3+/}Gd^{3-}$ doped HAp nanorods by F. Chen et al. [10] exhibited inappreciable *in vitro* cell toxicity and showed a high drug adsorption capacity and sustained ibuprofen release as a model drug, governed by a diffusion process. The cytotoxicity, drug adsorption and release, as well as in vitro/in vivo MR/luminescence/computed tomography (CT) imaging of Eu^{3+} and Gd dual doped HAp nanorods were also investigated by F. Chen et al. [10]. Recently, E. Boanini et al. [11] provided an overview of the recent results achieved on ion-substituted calcium phosphates prepared at low temperature by direct synthesis in aqueous medium or by hydrolysis of more soluble calcium phosphates. In recent years, C.S. Ciobanu et al. [12] reported a novel co-precipitation adapted synthesis for europium doped hydroxyapatite (Eu:HAp). They have synthesized europium-doped hydroxyapatite nanoparticles by co-precipitation method at low temperature and have shown by XRD studies that Eu^{3+} have been successfully inserted into HAp. Their results revealed that the obtained Eu:HAp ($x_{Eu} \geq 0$) particles are well assigned to the hexagonal lattice structure of the hydroxyapatite phase. On the other hand, their resultants showed the prepared Eu:HAp samples conserved regular ellipsoidal morphology and the doping with Eu^{3+} had little influence on their morphology.

The aims of this work concerns the study of the effects of Eu doping on a wide concentration range on the phisico-chemical properties of the Eu:Hap samples. The samples were characterized by various techniques including: transmission electron microscopy (TEM), BET and X-ray photoelectron spectroscopy (XPS). Up to now, the report on the comprehensive study in which a surface sensitive technique, XPS, has been not found.

On the other hand, we report for the first time the effects of europium-doped hydroxyapatite nanoparticles in terms of morphology and size in human kidney cells (HEK293) response regarding the actin cytoskeletal filaments disposition and heat shock proteins expression. Although it is well known that hydroxyapatite represents a mineral involved in osteogenesis, it is also responsible for nephrolithiasis [13] because an important percent of renal stones contain calcium phosphate in the form of hydroxyapatite [14]. Taking into account that the shape and dimension of hydroxyapatite nanoparticles are important parameters in the process of phosphate renal stones formation [15], this study aims to evaluate the renal cells response to the nanoscale particles synthesized by co-precipitation method.

2. Materials and methods

2.1 Synthesis of the samples.

Europium doped hydroxyapatite, $Ca_{10-x}Eu_x(PO_4)_6(OH)_2$ with $x_{Eu}=0$ (pure HAp), $x_{Eu}=0.01$, $x_{Eu}=0.02$, $x_{Eu}=0.2$ were synthesized by a co-precipitation method at 100^0C mixing $Eu(NO_3)_3 \cdot 6H_2O$, $Ca(NO_3)_2 \cdot 4H_2O$ and $(NH_4)_2HPO_4$ in deionized water in agreement with [12,16].

2.2 Characterization techniques.

Transmission electron microscopy (TEM) analyses were carried out using a JEOL 200 CX. The specimen for TEM imaging was prepared from particle suspensions in deionised water. A drop of well-dispersed supernatant was placed on a carbon – coated 200 mesh copper grid, followed by drying the sample at ambient conditions before it is attached to the sample holder on the microscope.

The functional groups present in the prepared nanoparticles and thin films were identified by FTIR using a Perkin Elmer Spectrum BX spectrometer. In order to obtain the nanoparticles spectra, 1% of the nano-powder was mixed and ground with 99% KBr. Tablets of 10 mm diameter were prepared by pressing the powder mixture with a pressure of not more than $0.69.10^5$ Pa. The spectrum was recorded in the range of 400 to 4000 cm^{-1} with 4 cm^{-1} resolution. The first FTIR spectra were obtained after 256 scans at room temperature (25 ± 0.5°C). The data interpretation was done according to [17-19].

X-ray photoelectron spectroscopy (XPS) measurements were carried out on a SPECS Multimethod Surface Analysis System using monocromatic Al Kα radiation (1486.6 eV). The vacuum in the analyzer chamber was $p \sim 3 \times 10^{-9}$ torr. The X-rays are emitted by an anti-cathode of Al, U = 12.5 kV, filament emission current I = 20 mA. For charge compensation a FG40 flood gun had been used, providing an electron beam of 2 eV and 0.3 mA. The XPS recorded spectrum involved an energy window w = 20 eV with the resolution R = 20 eV, and with 400 recording channels. The XPS spectra recorded were processed using Spectral Data Processor v2.3 (SDP) software. N_2 adsorption/desorption analysis was performed at 77 K using a Micrometrics model ASAP 2020 analyser. The specific surface area was determined by the Brunauer–Emmett–Teller (BET) method [20]. The pore parameters (pore volume and pore diameter) were evaluated from the desorption branch of the isotherm based on the Barrett–Joyner–Halenda (BJH) model [21]. The mean pore diameter, Dp, was calculated from Dp = 4VT/S [20], where VT is the total volume of pores, and S is the BET surface area.

2.3 Biological studies

2.3.1 Cell culture.

HEK 293 cell line (ATCC CRL-1573), derived from human embryonic kidney cells, was maintained in DMEM medium containing 10% fetal bovine serum, 100 U/ml penicillin and 100 µg/ml streptomycin, in a humidified atmosphere (5% CO_2) at 37^0C. The culture medium was changed every 2 days until cells reached confluence and then were trypsinized with 0.25% (w/v) Trypsin - 0.53 mM EDTA (Sigma-Aldrich).

2.3.2 F-actin staining.

HEK 293 cells were seeded onto six-well plates (3 x 104 cells/ well) and exposed to 100 µg/mL of 0%, 1%, 2% and 20% Europium doped hydroxyapatite. After 24 and 48 hours of treatment, the medium was removed, and the cells were fixed in 4% paraformaldehyde for 20 minutes at 4°C and permeabilized with 0.5% Triton X-100 for 1 hour. After three washes with PBS, the cells were incubated for 30 min in PBS containing 20 µg/mL phalloidin – FITC (Sigma-Aldrich). The nuclei were counterstained with 2 µg/mL DAPI (Invitrogen). The cells were observed using an Olympus IX71 fluorescent microscope with the excitation wavelengths set to 495 nm and 358 nm, and the emission wavelengths set to 513 nm and 461 nm for FITC and DAPI signal detection, respectively.

2.3.3 Western Blot analysis.

For determination of chaperones (Hsp60, Hsp70 and Hsp90) expression at protein level, Western blot analysis was performed. The cells were cultured in the presence of appropriate medium and after 24 or 48 hours of treatment (25 or 100 µg/mL of 0%, 1%, 2% and 20% Europium doped hydroxyapatite) were harvested in lysis buffer (150 mM NaCl, 1% Triton X-100, 0.5% sodium deoxycholate, 0.1% SDS, 50 mM Tris-HCl, pH 8.0 and protease inhibitor cocktail) and incubated for 30 min on ice. Cell lysates were clarified by centrifugation at 13,000 g for 20 min and supernatants collected were boiled (95^0C) for 5 min. Equal amounts of total

protein were subjected to SDS-polyacrylamide gel electrophoresis. Proteins were transferred to Hybond-PVDF membranes in Tris-glycine buffer (48 mM Tris-HCl, pH 8.3, 39 mM glycine, 20% methanol) using a wet transfer unit (BIO-RAD, USA), and after that, membranes were blocked overnight at 4°C, and incubated with specific mouse monoclonal IgG anti-HSPs (all from Santa Cruz Biotechnology) and anti-β-actin (from Sigma-Aldrich). The Western Blot Chromogenic Immunodetection Kit (INVITROGEN) which contains secondary antibody anti-mouse IgG conjugated with alkaline phosphatase and BCIP/NBT substrate for alkaline phosphatase were used according to manufacturer's instructions. Densitometry data were analyzed by GelQuantNET software for semi-quantification of HSPs and beta-actin.

Whole cell lysates of control (Ctrl) and europium-doped hydroxyapatite treated cells were separated on 10% SDS-PAGE, transferred to PVDF membrane that was incubated with anti-Hsp60, anti-Hsp70 and anti-Hsp90 antibodies.

β-actin expression was used as a loading control. One representative blot was figured for 24 and 48 hours of treatment (A). The densities of HSPs bands were measured and the content was normalized against β-actin. Results indicate the percentage of control group. Values are shown as mean ± S.D. from three independent experiments, each performed in triplicate.

Statistical analysis. All experiments were done in triplicate and measurements repeated at least three times. The results w ere expressed as percent of the control values. Data are represented as mean ± standard deviation.

3. Results

3.1 Structure, formation and morphology of pure HAp and Eu:Hap

The crystal structure of the prepared samples was verified by X-ray diffraction (XRD) [12]. The XRD patterns of the Eu:HAp, $Ca_{10-x}Eu_x(PO_4)_6(OH)_2$, with different x_{Eu} values (x_{Eu}=0.01, 0.02 and 0.2) and HAp (x_{Eu}=0) confirmed the hexagonal lattice symmetry (space group P63/m) for all samples. In previous studies [12-22] it was shown that all the XRD patterns of Eu:HAp samples and pure HAp can be well indexed as a hexagonal phase agreeing well with the values of the standard ASTM data (JCPDS no. 9-0432) indicating a moncrystalline hydroxyapatite phase. Fig. 1 displays the HRTEM images and Selected Areas Electron Diffraction (SAED) of Eu:HAp nanoparticles with x_{Eu} = 0.02 and confirms that the synthesized samples are well-crystallized even at small values of x_{Eu}. In the HRTEM image (Fig. 1 B) it can be seen that the crystalline phase of hydroxyapatite with well-resolved lattice fringes can be observed. The distances (2.81Å and 1.84Å) between the adjacent lattice fringes is in accordance with the d211and d213 spacing values reported in literature (0.2814 nm and 0.184 nm) (JCPDS no. 09-0432). The HRTEM images of the sample further confirm that the synthesized samples are well crystallized single crystals.

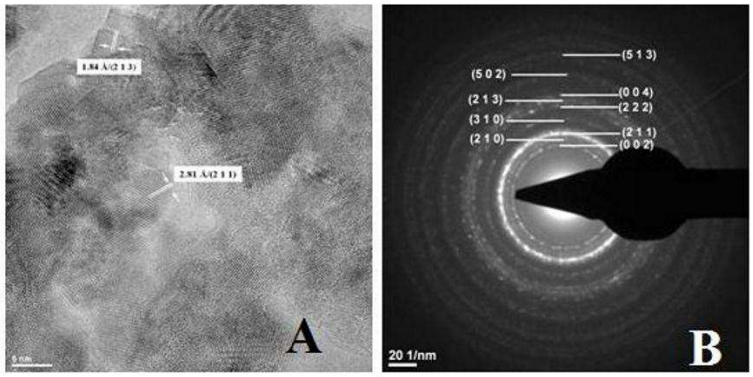

Figure 1. HRTEM image of Eu:HAp with x_{Eu}= 0.02.

In the 4000 cm^{-1} to 400 cm^{-1} range, in Fig. 2, are shown the IR absorbance spectra of Eu:HAp samples with various europium concentrations ($0 \leq x_{Eu} \leq 0.2$).

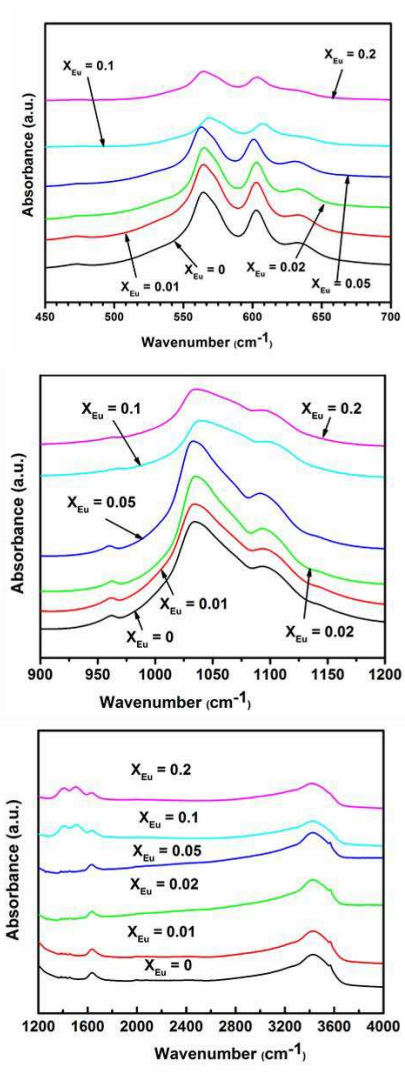

Figure. 2. FTIR spectra of europium doped hydroxyapatite (Eu:HAp) with x_{Eu}=0 (black), x_{Eu}=0.01 (red), x_{Eu}=0.02 (green), x_{Eu}=0.05 (dark blue), x_{Eu}=0.1 (light blue) and x_{Eu}=0.2 (purple).

In our previous studies [23] we have shown that for all the samples the presence of strong OH^- vibration peak (632 cm^{-1}) could be noticed. The presence of the broad bands of adsorbed water in the regions 1600–1700 cm^{-1} and 3200–3600 cm^{-1} are due to characteristic OH^- modes (Figure 2). Furthermore, in the last studies on apatites [24] has been reported that the band at 3570 cm^{-1} (stretching) is characterized by OH^- vibrational mode and the band at 632 cm^{-1} characterized by OH^- arises from stretching librational mode.

In agreement with A. Slosarczyk et al. [25] the most noticeable feature in these spectra concerns the presence of the typical ν_4 PO_4^{3-} and ν_3 PO_4^{3-} IR vibrations of phosphates group belonging to apatite in the range from 530–650 cm^{-1} and 900–1200 cm^{-1} respectively [26]. The bands at around 1090 cm^{-1} and about1040 cm^{-1} can be attributed to the ν_3 PO_4 while the band at 962 arises from ν_1 PO_4. The 602 cm^{-1} and 564 cm^{-1} bands appear from ν_4 PO_4. Markovik et al. [27], presented that the sharpness of bands, especially sharpness of the 632 cm^{-1}, 602 cm^{-1} and 564 cm^{-1} bands indicate a well-crystallized HAp. The band at 475 cm^{-1} can be attributed to the ν_2 PO_4.

On the other hand, in the second derivative spectra the band at 475 cm^{-1} was identified a $\nu_2(PO_4^{3-})$. In concordance with precedent studies [23, 28], the bands assigned in the second derivative spectra of Eu:HAp ($0 \leq x_{Eu} \leq 0.2$) can be attributed to molecular vibrations of the phosphate (PO_4^{3-}) in a apatitic stoichiometric environment of hydroxyapatite [28].

In the FT-IR spectrum of Eu:HAp with $x_{Eu} \geq 0.1$ (Fig. 2) the bands corresponding to the ν_3 vibration of C–O were observed at 1410 cm^{-1}, characteristic of the carbonate group [29-30].

The intensity of the band located at 1410 cm^{-1} in the spectrum of Eu:HAp samples with $x_{Eu} \geq 0.1$ is attributed to components of the ν_3 mode of a trace amount of CO_3^{2-}. The ν_2 vibrations between 850 and 890 cm^{-1}, characteristic of the carbonate group were not detected because ν_2 CO_3 band at 872 cm^{-1} is hidden by HPO_4 band at 875 cm^{-1}. Similar comportment was observed by M. Markovik et al. [27] in his studies on preparation and comprehensive characterization of calcium hydroxyapatite. M. Markovik et al. and D.W. Holcomb et al. [31] showed that the CO_3 band at 1410 cm^{-1} derives from CO_3^{2-} (designated by "B-type" carbonate that replace PO_4^{3-} ions in the hydroxyapatite lattice). The band at 1510 cm^{-1} was also detected in the FT-IR spectrum of Eu:HAp with $x_{Eu} \geq 0.1$. The band at 1510 cm^{-1} derives from CO_3^{2-} (designated by "A-type" carbonate) that replaces OH^- ions in the hydroxyapatite lattice [27, 32]. In all the spectra of Eu:HAp samples, the band at 875 cm^{-1} was detected. This band is supposed to arise due to HPO_4^{2-} ions from several reasons [27].

In order to investigate the successful doping of Eu in Eu:Hap, X-ray photoelectron spectroscopy (XPS) measurements were performed. High resolution spectra of the C 1s, Ca 2p, P 2p, O 1s and Eu 3d regions were obtined.

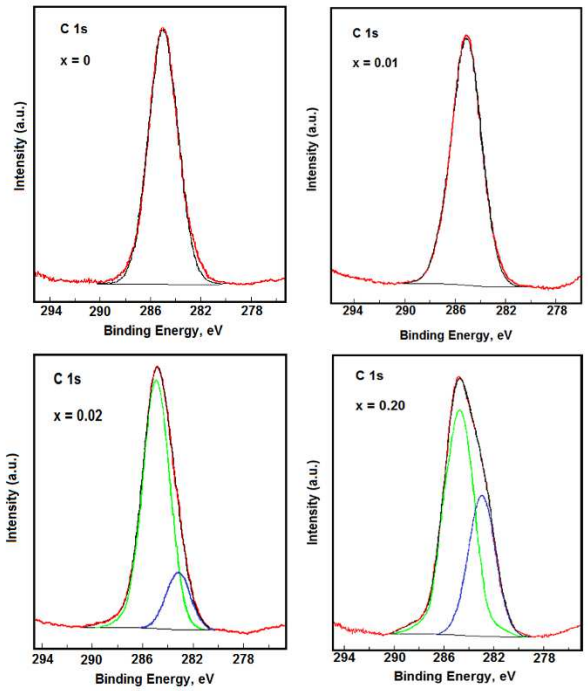

Figure 3. High-resolution XPS spectra and curve-fitting results of carbon C 1s for Eu:HAp (x_{Eu}=0.01, x_{Eu}=0.02, x_{Eu}=0.2) and pure HAp (x_{Eu}=0) samples.

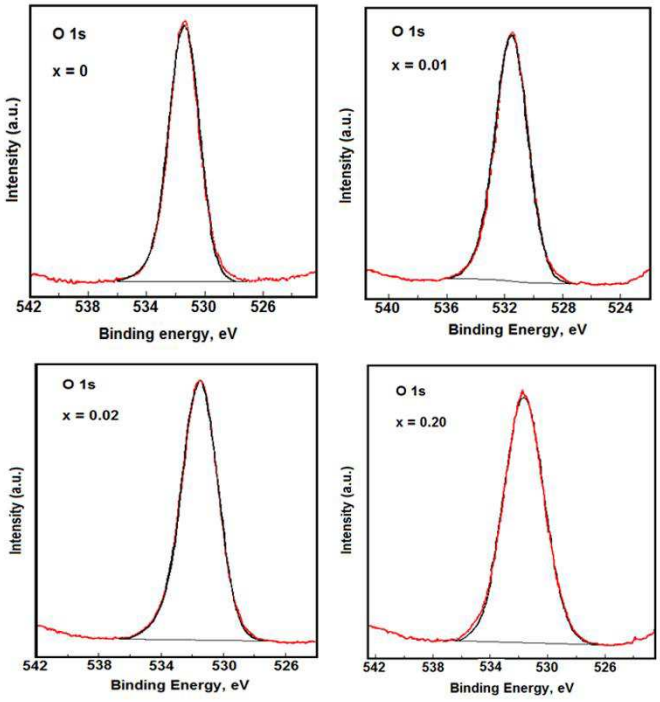

Figure 4. High-resolution XPS spectra and curve-fitting results of oxygen O 1s for Eu:HAp (x_{Eu}=0.01, x_{Eu}=0.02, x_{Eu}=0.2) and pure HAp (x_{Eu}=0) samples.

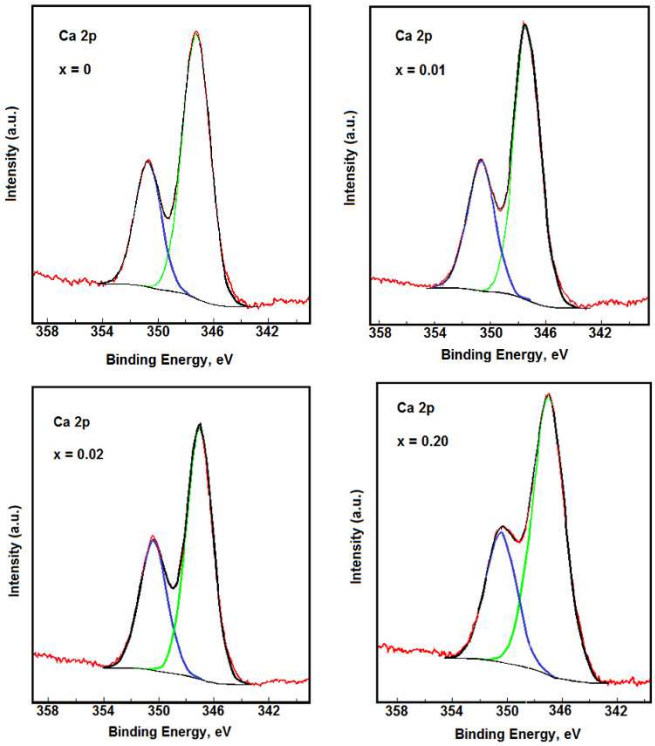

Figure 5. High-resolution XPS spectra and curve-fitting results of calcium Ca 2p for Eu:HAp (x_{Eu}=0.01, x_{Eu}=0.02, x_{Eu}=0.2) and pure HAp (x_{Eu}=0) samples.

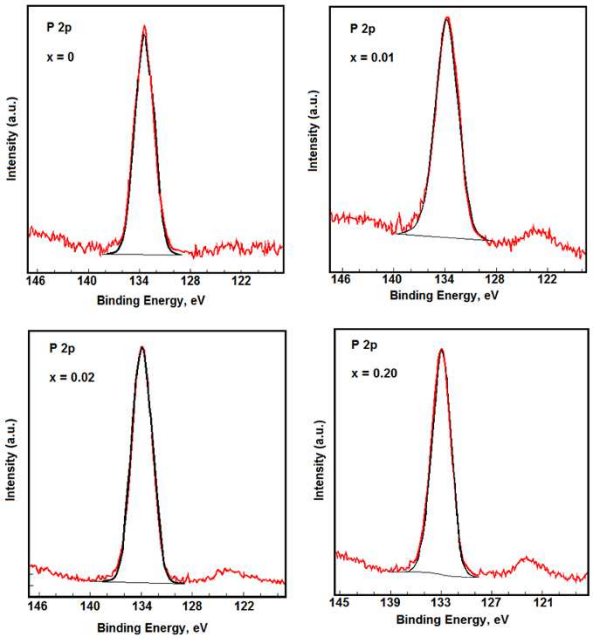

Figure 6. High-resolution XPS spectra and curve-fitting results of phosphorous P 2p for Eu:HAp (x_{Eu}=0.01, x_{Eu}=0.02, x_{Eu}=0.2) and pure HAp (x_{Eu}=0) samples.

The measured binding energy (E_B) scale was referenced to a C 1s at the E_B value of 284.8 eV [33]. Figure 3 shows the high–resolution C 1s spectra for the Eu:HAp (x_{Eu}=0.01, x_{Eu}=0.02, x_{Eu}=0.2) and pure HAp (x_{Eu}=0) samples. Decomposition of multiple peaks in the C 1s region was performed and each spectrum had a shoulder on the higher-binding-energy side in addition to the main peak around 284.8 eV. For the samples with x_{Eu}=0.02 and x_{Eu}=0.2 a new peak is observed at around 283.4 eV. The peaks at 284.8 eV and 283.4 eV correspond to residual or adventitious carbon. In the opinion of J. Serra et al. [34] the peak positioned at 284.8 eV, corresponds to C–C and C–H bonds.

The peak positioned at 283.4 eV could correspond to C-metal bonds, showing a chemical interaction between Eu and contaminants from surface layer. The O 1s, Ca 2p, P 2p photoelectron peaks were decomposed according to the binding energies of carbon bonds in hydroxyapatite [35-36].

Figure 4 shows the high resolution XPS spectra of oxygen O 1s for Eu:HAp, $Ca_{10-x}Eu_x(PO_4)_6(OH)_2$, with different x_{Eu} values and pure HAp. The peak from 531.4 eV corresponds to hydroxyl groupings resulting from the chemisorption of water or oxygen. These results are in accordance with previous studies of J.F. Moulder et al. [37]. The peak position of the hydroxyl ion (OH^-) was reported as E_B=531.8 eV on a SnO_x surface [38]. On the other hand, T. Kawabe et al. [39] consider that two oxygen species, i.e., O^- and OH^-, may be included in the resolved peak at 531.2 eV. Furthermore, the peak position of chemisorbed oxygen species O^- on nickel was reported as binding energy, E_B=531.0-531.5 eV [40-42]. Figure 5 presents the high-resolution Ca 2p spectra for Eu:HAp (x_{Eu}=0.01, x_{Eu}=0.02, x_{Eu}=0.2) and pure HAp (x_{Eu}=0) samples. The Ca 2p band of the as-prepared samples exhibits a well-resolved doublet with a Ca $2p_{3/2}$ component and a Ca $2p_{1/2}$ component. Increasing the europium concentration, the binding energies shift slightly from 347.2 eV for the pure HAp (x_{Eu}=0) to 347.7 eV for the Eu:HAp (x_{Eu}=0.2). The peak located at about 347.2 eV shows that the calcium atoms are bonded with a phosphate group (PO_4^{3-}). Moreover, S. Kaciulis et al. have shown [43] that the shift towards higher binding energy for the Eu:HAp samples indicates that the amount of crystalline HAp has increased.

After the deconvolution data processing, the P 2p photoelectron line consists of one single peak, at around E_B=133.1eV for pure HAp (x_{Eu}=0) and Eu:HAp (x_{Eu}=0.01, x_{Eu}=0.02 and x_{Eu}=0.2) samples [44]. The high-resolution XPS spectra and curve-fitting results of phosphorous P 2p for Eu:HAp and pure HAp samples are exhibited in Figure 6. T.F. Stoica et al. showed [45] that the P 2p photoelectron line consists of one single peak at E_B position of 133.4 eV. Moreover, in agreement with previous XPS studies reported [46], the binding energy of the photoelectron peaks for Ca and P are characteristic to their full oxidation states (Ca^{2+} and P^{5+}) for hydroxyapatite.

The high-resolution XPS spectra of the Eu 3d region (Figure 7) shows the presence of europium in the form of Eu^{3+} in Eu:HAp (x_{Eu}=0.01, x_{Eu}=0.02, x_{Eu}=0.2) samples. For Eu $3d_{3/2}$ the peak appears at a binding energy of 1136.5 eV. These results indicate that europium ions were successfully incorporated into the HAp lattice. The Ca/P ratios were 1.67 of the nanocrystalline pure HAp (x_{Eu}=0) and 1.64 of europium doped hydroxyapatite (Eu:HAp). In agreement with J. Nathanael et al., [47] the decrease of Ca/P ratio in the Eu:HAp can obviously be linked to the substitution of Ca ions by Eu ions.

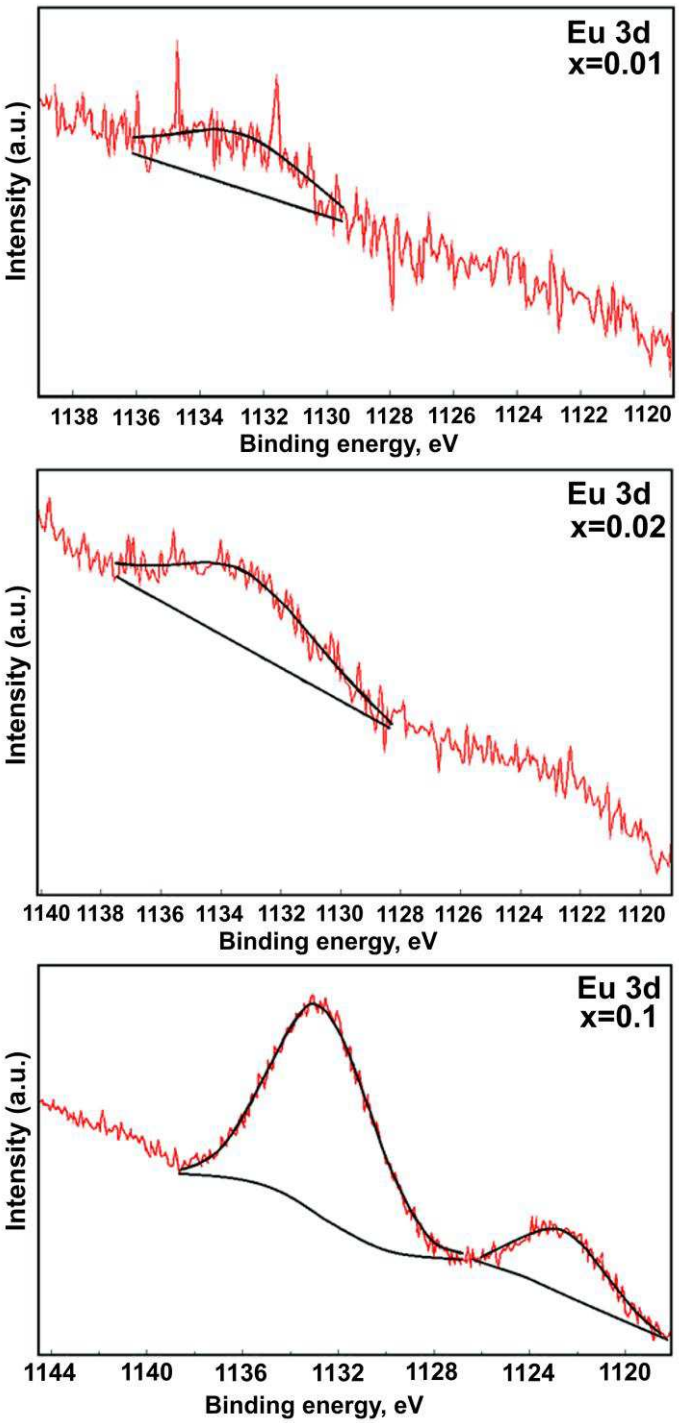

Figure 7. High-resolution XPS spectra and curve-fitting results of phosphorous Eu 3d for Eu:HAp (x_{Eu}=0.01, x_{Eu}=0.02, x_{Eu}=0.2) samples.

Porosity of Eu:HAp and pure HAp samples were measured using the nitrogen physisorption technique. Figure 8 shows the representative adsorption–desorption isotherms of the Eu:Hap with different x_{Eu} values (x_{Eu}=0.01, 0.02 and 0.2) and HAp (x_{Eu}=0). All the samples show

isotherms of type IV [48], with a hysteresis loop at a relative pressure (P/P_0) between 0.4 and 1.0, indicating the presence of mesopores. For all the samples the shape of the hysteresis loop is of type H1 which demonstrates the properties of typical mesoporous materials [49].

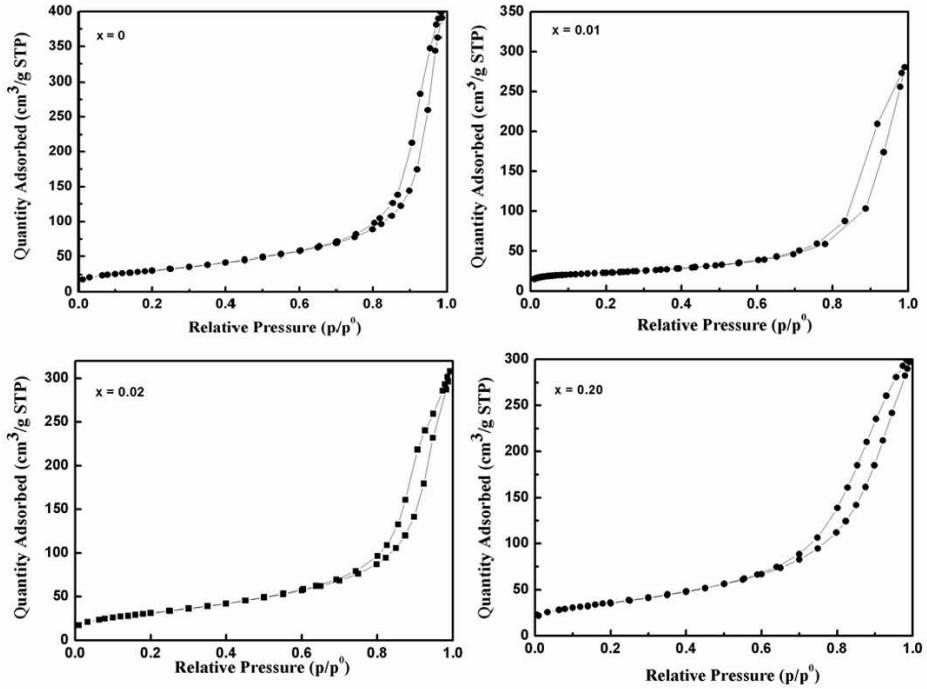

Figure 8. N_2 adsorption–desorption isotherms of Eu:HAp (x_{Eu}=0.01, x_{Eu}=0.02, x_{Eu}=0.2) and pure HAp (x_{Eu}=0) samples.

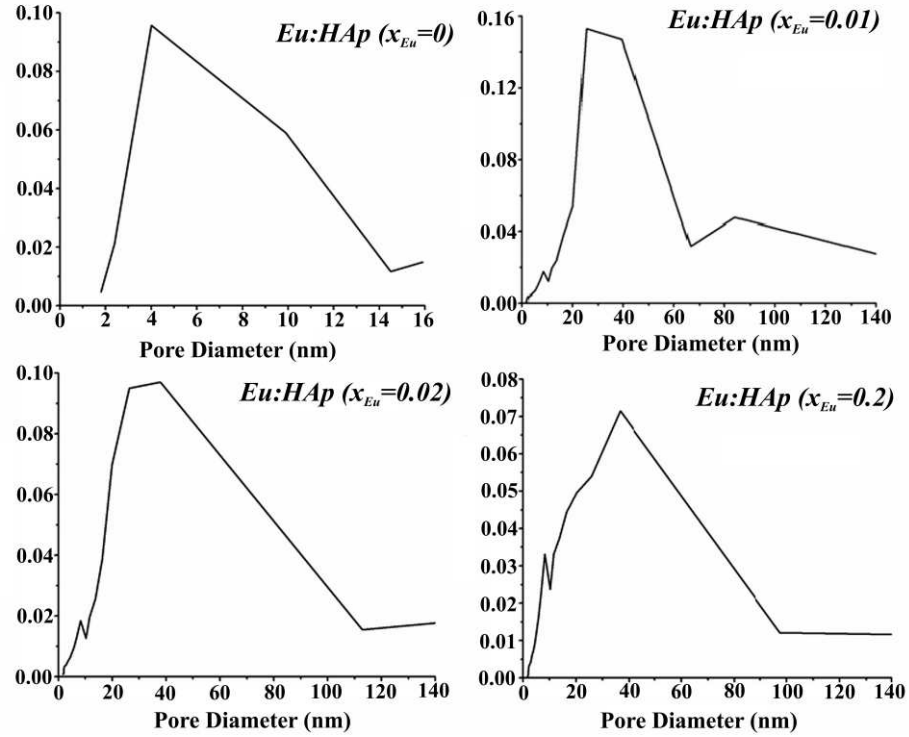

Figure 9. Pore size distribution of Eu:HAp (x_{Eu}=0.01, x_{Eu}=0.02, x_{Eu}=0.2) and pure HAp (x_{Eu}=0) samples.

In accord with [50-51], these mesopores are usually formed due to the agglomeration of primary crystallites. As shown in Figure 8, the order of BET specific surface areas and Langmuir specific surface areas are as follows: Eu:HAp (x_{Eu}=0.2) > Eu:HAp (x_{Eu}=0.02) > Eu:HAp (x_{Eu}=0.01)>HAp (x_{Eu}=0). The pore size distributions measured using the BJH method is presented in Figure 9. The maximum BET surface area, Langmuir surface area, and the maximum pore volume obtained were 130.21 m^2/g, 192,091m^2/g and 0.49 cm^3/g, respectively for the samples of Eu:HAp with x_{Eu}=0.2. The average pore diameter value, Dp, increases from 5.61 to 7.83 nm when x_{Eu} increases. The properties of the tested samples are summarized in Table 1.

Table 1. BET surface area, Langmuir surface area, pore size and pore volume of Eu:HAp samples and pure HAp.

Samples	x_{Eu}	BET surface area (m^2/g)	Langmuir surface area (m^2/g)	Pore size (nm)	Pore volume (cm^3/g)	D_p (nm)
Eu:HAp	0.01	112.90	167.72	22.04	0.43	5.07
	0.02	115.96	171.26	16.56	0.48	5.61
	0.20	130.21	192.091	14	0.49	6.74
HAp	0	71.88	107.27	24.36	0.41	7.83

3.2 Biological studies

Our previous biocompatibility studies of Eu doped crystalline hydroxyapatite bioceramics [22] showed no significant decrease of viability of the HEK293 cell line and low levels of intracellular lipid peroxidation in the Eu-doped HAp treated cells. In order to visualize how Eu-doped hydroxyapatite influences the adhesion and proliferation of HEK293 cells, a phalloidin-FITC staining for F-actin was performed. F-actin is a highly conserved and abundant cytoskeletal protein in eukaryotic cells. It is implicated in maintaining the cellular architecture and mediating cell movements [52]. As shown in Figure 10 and 11, the cell proliferation was not affected after 24 or 48 hours of Eu-doped HAp exposure. The cells adopted a normal morphology, each having contact with the surrounding cells.

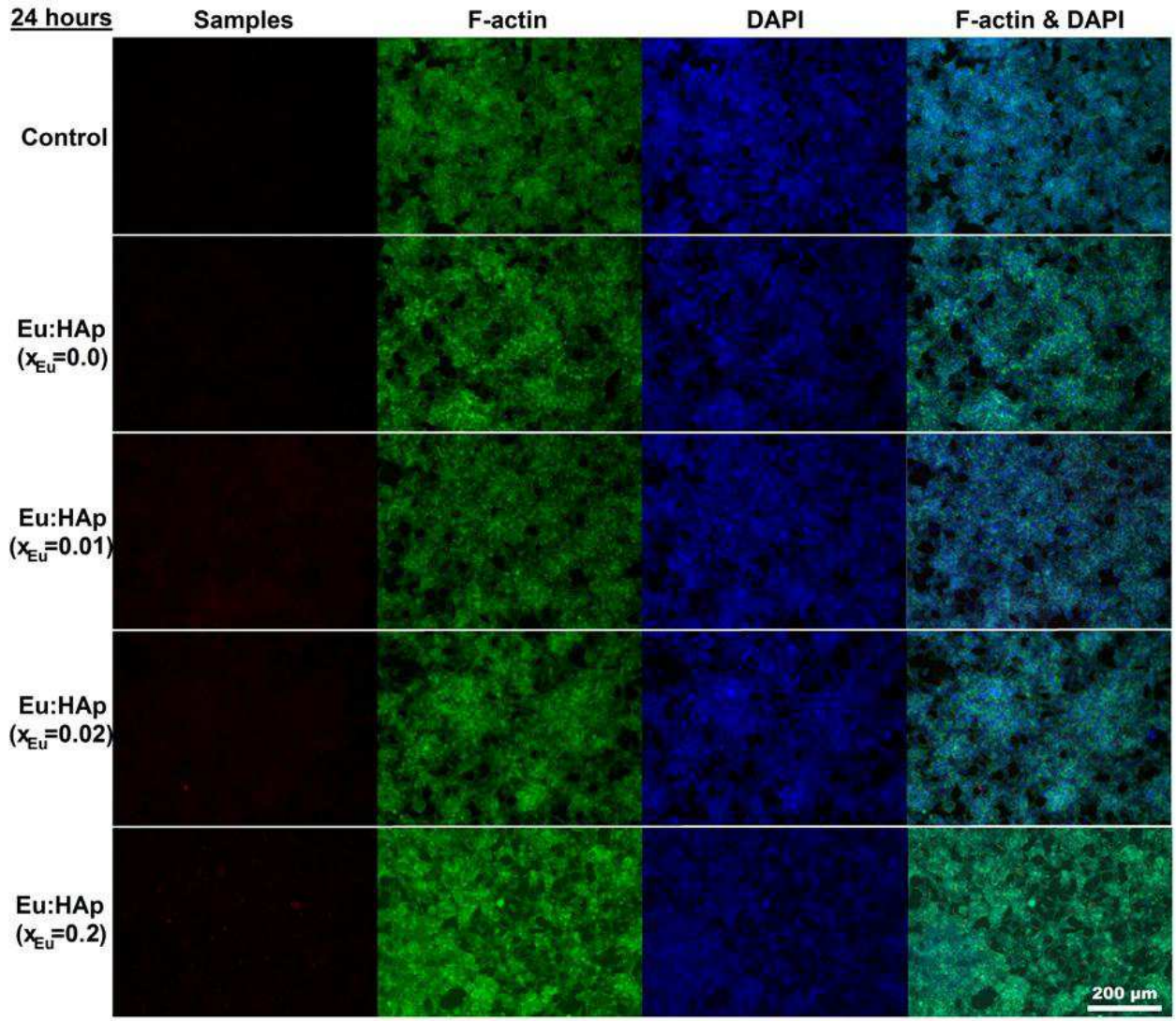

Figure 10. Fluorescence images of HEK293 cells cultured in the presence of 100 µg/mL of Eu:HAp (x_{Eu}=0.01, x_{Eu}=0.02, x_{Eu}=0.2) for 24 hours. Actin cytoskeleton of cells, stained with phalloidin-FITC (green), shows a apropriate morphology. The nuclei were counterstained with DAPI (blue).

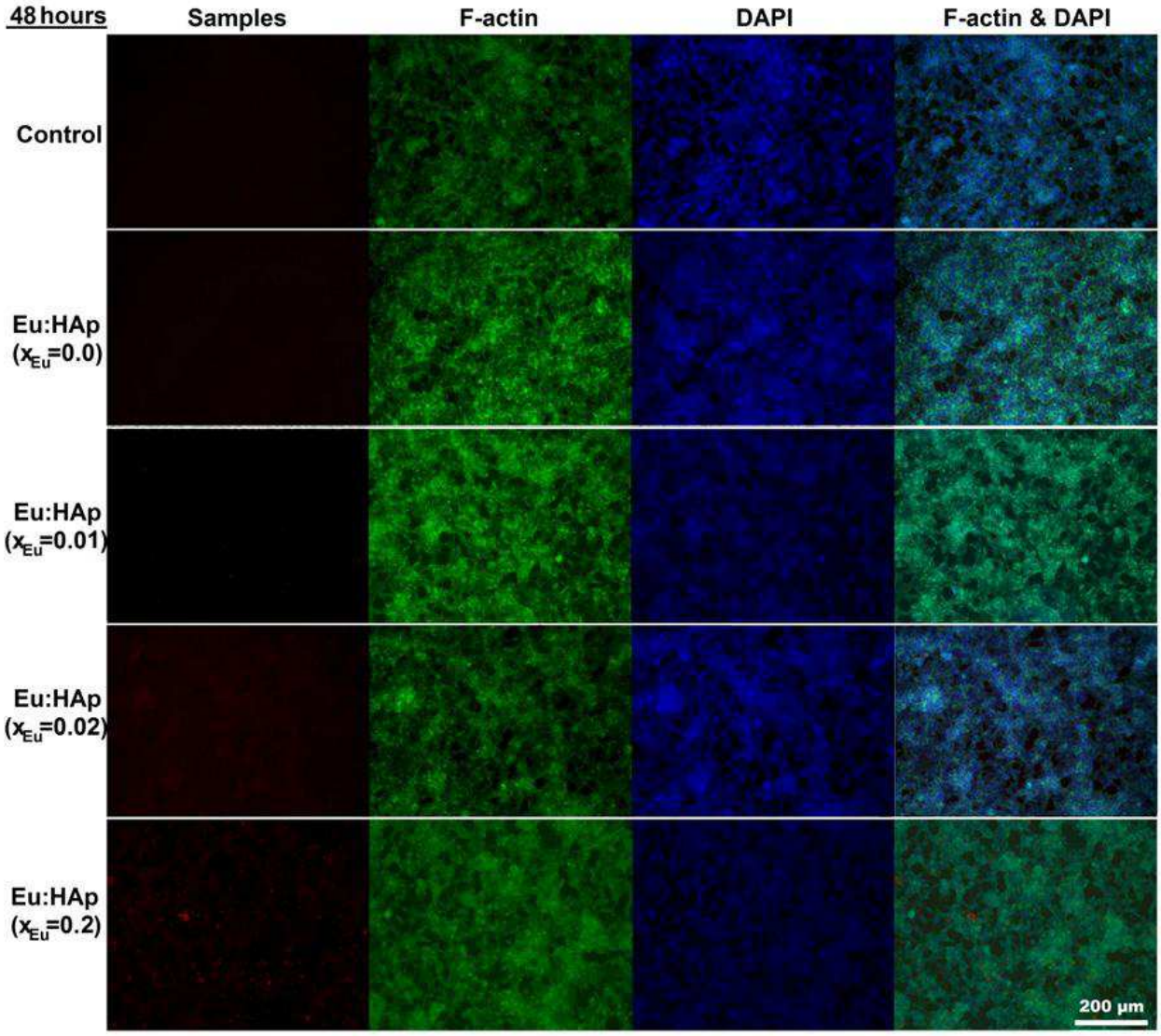

Figure 11. Fluorescence images of HEK293 cells cultured in the presence of 100 µg/mL of Eu:HAp (x_{Eu}=0.01, x_{Eu}=0.02, x_{Eu}=0.2) for 48 hours. Actin cytoskeleton of cells, stained with phalloidin-FITC (green), shows a appropriate morphology. The nuclei were counterstained with DAPI (blue).

It is notably that the cells are not disturbed by the presence of this type of hydroxyapatite, maintaining a healthy morphology and good adhesion. Moreover, it can also be remarked that the proliferative capacity of these cells was not affected compared to control cells.

Heat shock proteins, Hsp60, Hsp70 and Hsp90 are molecular chaperones, and their expression is unregulated under many kinds of stresses, such as heat or chemical toxicity [53].

As shown in Figure 12, cells exposed to different types and concentration of Eu doped HAp showed no important modifications of Hsp60, Hsp70 and Hsp90 expression compared to control cells.

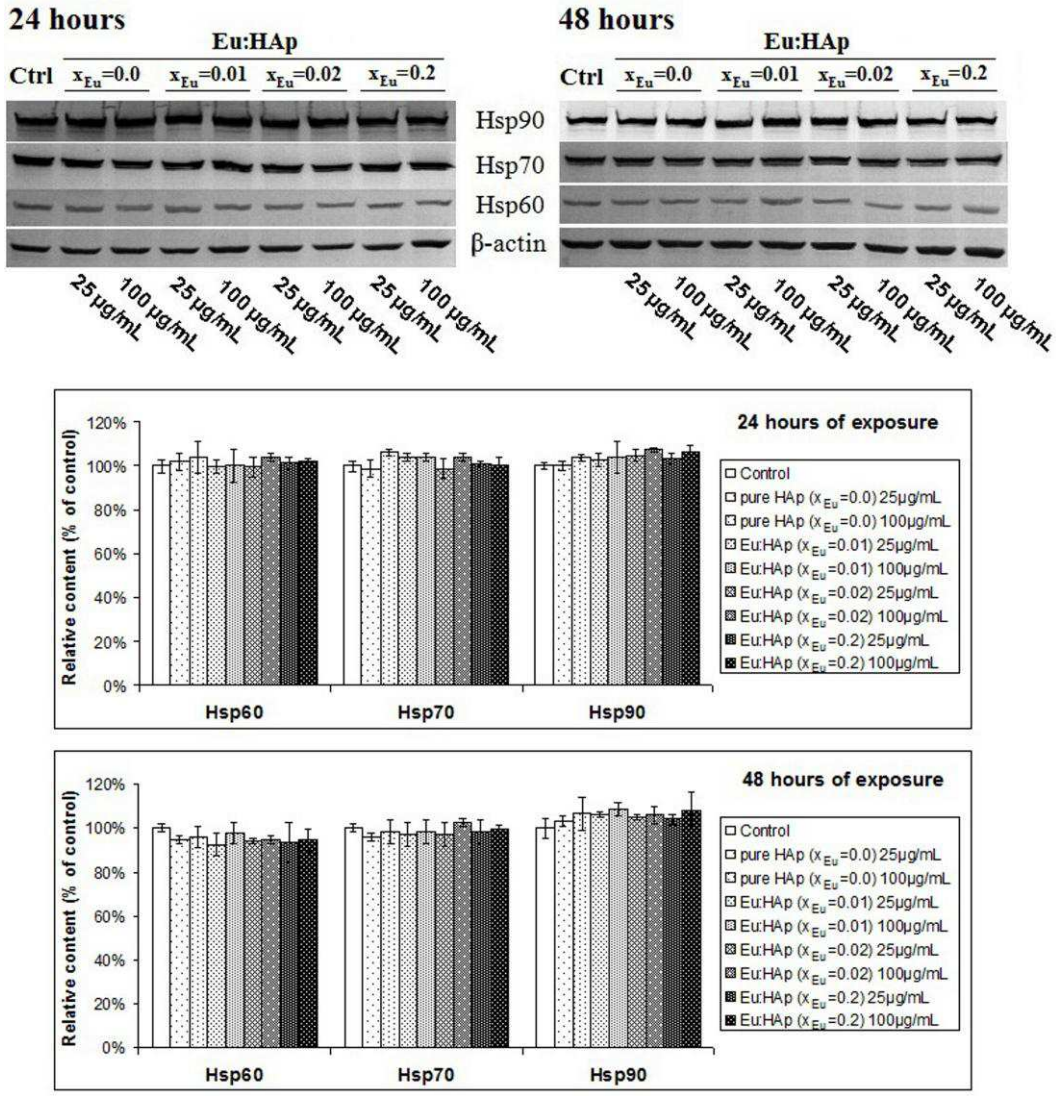

Figure 12. Western blot analysis of Hsp60, Hsp70 and Hsp90.

4. Discussion

Hydroxyapatite presented in the recent years a significant interest for different fields such as pharmaceutics or biological and medical diagnostics [9, 54] due to the biocompatible and osteoconductive properties [55-56]. Based on the flexibility of the apatitic structure, HAp can incorporate a wide variety of substitutions for Ca^{2+}, PO_4^{3}, and/or OH^- ions [57-61]. Since Eu^{3+} has a similar ionic radius to Ca^{2+}, HAp is a good host for Eu^{3+}. The substitution of Ca^{2+} by a Eu^{3+} ion has been achieved by various methods of synthesis such as solvothermal method [62], a combination of sol–gel and electrospinning processes [63]. R.S. André et al. [8] obtained Eu-doped hydroxyapatite nanorods by HTMW method at 140°C for 0, 1, 20 or 40 min. On the other hand, based on the flexibility of the apatitic structure I.R. Gibson et al. [64] has prepared by aqueous precipitation method the silicon-substituted hydroxyapatite.

For this study, we synthesized the mesoporous and luminescent europium doped hydroxyapatite (Eu:HAp) powders with different concentration (x_{Eu}=0, x_{Eu}=0.01, x_{Eu}=0.02,

x_{Eu}=0.2) by co-precipitation method at low temperature. Our previous XRD studies [12, 22] have shown that no other secondary phase such as calcium carbonate and/or europium oxide can be detected in XRD patterns. The results of XRD studies indicated that pure Eu:HAp nanoparticles were obtained by simple co-precipitation method. The HRTEM images and Selected Areas Electron Diffraction (SAED) of Eu:HAp nanoparticles confirms that the synthesized samples are well-crystallized single crystals even at small values of x_{Eu}.

In FTIR analysis we observed that the contribution of the area that corresponds to the phosphate bands decreases when the Eu concentration in the samples increases. The bands at 475 and 962 cm^{-1} progressively disappear with the increase of europium concentration. When the x_{Eu}=0.2 the bands at 475 and 962 cm^{-1} are almost absent. We can also observe in the Eu:HAp spectra a broadening of peak vibration with the decrease of the europium concentration. This behaviour was also observed by H. Owada et al. [65] in sintered Y-doped hydroxyapatite.

The XPS results of the surface composition of the studied samples are according to the previous result obtained by C. Yang et al. [62]. This is the first comprehensive study in which a surface sensitive technique, XPS, has been employed to confirm the substitution of Ca^{2+} by Eu^{3+} into HAp. The analysis showed that when europium is present (Eu:HAp) the binding energies of Ca, P and O do not change when compared to the ones of pure HAp (x_{Eu}=0). On the other hand, the changes in the atomic percentages of the elements suggest a possible substitution of Ca by Eu. Regarding the Ca2p, P2p and O1s bands, there was no noticeable variation of their position when europium is present. The XPS results show that the P/O ratio remains relatively constant, the Ca/P ratio decreased while the Eu/Ca ratio increased. The (Ca+Eu)/P ratio obtained for the Eu:HAp (x_{Eu}=0.01, x_{Eu}=0.02, x_{Eu}=0.2) sample is practically the same as the Ca/P ratio of pure HAp (x_{Eu}=0). The fact that the ratio P/O is relatively constant in all the samples indicates that there was little or no loss of phosphate from the surface.

The results of the nitrogen adsorption/desorption analysis indicates that the doping of Eu^{3+} has not altered the basic pore structure of the mesoporous HAp but improved the specific surface area of about 60% for low concentration to 100% to the highest concentration of Eu.

Furthermore, in our study it can be noticed that in the cells treated with different types and concentrations of Eu doped HAp nanoparticles for 24 h and 48 h, F-actin distribution was around the nuclei and extended until the periphery of HEK 293 cells, which is in accordance with previous data [66-67]. The F-actin pattern was the same for control and exposed cells, which suggested a very low or a lack of toxicity of these types of nanoparticles.

The induction of stress response proteins is highly conserved and protects different cells against several types of stressors [68]. Among the various stress response pathways, the gene expression and synthesis of different heat shock protein family members, such as Hsp 60, Hsp70 and Hsp 90, are some of the key processes [69]. In non-stressed conditions, these proteins function as molecular chaperones, maintaining and facilitating the protein conformation and transport. In response to stress, heat shock proteins expression counteracts protein aggregation, promotes the degradation of highly denatured proteins and refolds the misfiled proteins or with damaged three dimensional structure [70].

The Hsp70 chaperone systems play an essential role in hostile environments as well as under normal conditions. These are the most highly conserved and first to be induced in the presence of stressors [71]. The increased levels of Hsp70 have been considered as resulting due to the action of xenobiotics and/or their metabolites which have not been scavenged by detoxification processes and have affected the three dimensional structure of native proteins [72]. Several studies revealed that metal based nanoparticles induced toxicity in a cell type dependent

manner and the protein expression of Hsp70 was up-regulated [73-74]. Members of Hsp70 are found in the cytosol, nucleus, endoplasmic reticulum and mitochondrion [75]. In mitochondria, are also located mainly the members of Hsp 60 family proteins, coded by the nuclear genome, which play a significant role in polypeptide folding and in protein translocation [76].
In the same time, Hsp90 is the most abundant cytosolic heat shock protein family in eukaryotic cells and a decrease in its concentration is correlated with mortality in mammalian cells [71]. Recently, an increase of Hsp90 expression was noticed when melanoma targeted magnetite nanoparticles conjugated with a melanogenesis substrate were used [77].

Previous studies reported that in the cells exposed to hydroxiapatite based nanoparticles, a stress was developed [78-79]. This could be counteracted by an up-regulation of Hsps expression [74, 77]. Contrary to these observations, our study revealed no significant alteration of Hsp60, Hsp70 and Hsp90 expression.
Based on the direct correlation between the level of stress and the protein expression of Hsps, it seems that the level of toxicity induced in HEK 293 cells by the exposure to these nanoparticles was low or absent. These results were valid for all concentrations of Eu doped HAp tested in this study and were not europium level dependent.

5. Conclusion

The results presented in this paper show the influence of the europium doping on hydroxyapatite bioceramics prepared by the co-precipitation method. XPS analysis indicated that Eu was able to quickly substitute Ca into the HAp by a co-precipitation method. High-resolution XPS analysis of the key elements of as-prepared samples, Ca, P, O and Eu indicated that distinctive photoelectron peaks could be attributed to the presence of Eu in the as-prepared samples with x_{Eu}=0.01, x_{Eu}=0.02, x_{Eu}=0.2. Europium did not change the chemistry or morphology of the pure HAp. After the europium doped hydroxyapatite the BET specific surface area of the as-prepared samples increased from pure HAp to Eu:HAp with x_{Eu}=0.20. The as-prepared Eu:HAp samples exhibit mesoporous structure. The samples with a mesoporous structure are suitable for the drug delivery systems.

The lack of cytotoxic effect on actin organisation and no stress response initiation in cells were highlighted. It seems that the cell compatibility with these Eu:HAp bioceramics correlates very well with its structure and nano dimension.

Taken together, the normal aspect of F-actin filaments organization and heat shock proteins expression that remained almost unchanged support the idea that these Eu-doped HAp samples were not toxic and provided good conditions for cell proliferation. These sustain the applicability of europium-doped hydroxyapatite for medical purposes.

Acknowledgments

The authors would like to thank Dr. F. Frumosu for XPS measurements and Dr. B.S. Vasile for TEM measurements.

References

[1] R. Cortesi, C. Nasturzzi, S.S. Davis, Biomaterials 19, 1641 (1998).
[2] P. Yang , Z. Quan, C. Li , X. Kang , H. Lian , J. Lin, Biomaterials 29, 4341(2008).
[3] S.L. Iconaru, A.M. Prodan, P. Le Coustumer, D.Predoi, Journal of Chemistry doi:10.1155/2013/412079.

[4] C.S. Ciobanu, S.L. Iconaru, P. Le Coustumer, L.V. Constantin, D. Predoi Nanoscale Res. Lett. 7, 324 (2012**)**.
[5] C.S. Ciobanu, S.L. Iconaru, I. Pasuk, B.S. Vasile, A.R. Lupu, A. Hermenean, A. Dinischiotu, D.Predoi, Mater. Sci. Eng. C 33(3), 1395 (2013**)**.
[6] A.M. Beshensky, J.A. Wesson, E.M. Worcester, J. Am. Soc. Nephrol. 12, 2108 (2001).
[7] A. Doat , M. Fanjul , F. Pellé , E. Hollande , A. Lebugle, Biomaterials 24, 3365 (2003**)**.
[8] R.S. André, E.C. Paris, M.F.C Gurgel, I.L.V. Rosa, C.O. Paiva-Santos, M.S. Li, J.A. Varela, E. Longo, J. Alloys Compd. 531, 50 (2012**)**.
[9] C.A. Barta , K. Sachs-Barrable , J. Jia , K.H. Thompson , K.M. Wasan , C. Orvig , Dalton Trans. 21(43), 5019 (2007**)**.
[10] F. Chen , P. Huang , Y.J. Zhu , J. Wu , C.L. Zhang , D.X. Cui , Biomaterials 32, 9031 (2011**)**.
[11] E. Boanini, M. Gazzano, A. Bigi, Acta Biomater. 6, 1882 (2010**)**.
[12] C.S. Ciobanu, S.L. Iconaru, F. Massuyeau, L.V. Constantin, A. Costescu, D.Predoi, J. Nanomater. doi:10.1155/2012/94280 (2012).
[13] H.G. Tiselius, I. Hojgaard, A.M. Fornander, M.A.Nilsson, In Urolithiasis, (Millet the Printer Inc., Dallas, 1996).
[14] N.S. Mandel, G.S.Mandel, J. Urol. 142, 1516 (1989**)**.
[15] M. Zelenková, O. Sohnel, F. Grases, Urology 79(4), (2012).
[16] C. S. Ciobanu, E. Andronescu, B. S. Vasile, C. M. Valsangiacom, R. V. Ghita, D. Predoi, J. Optoelectron Adv. Mat. 4(10), 1515 (2010)
[17] J. Kolmas, A. Jaklewicz, A. Zima, M. Bućko, Z. Paszkiewicz, J. Lis, A. Ślosarczyk, W. Kolodziejski, J. Mol. Struct. 987, 40 (2011**)**.
[18] B. Matsuhiro, P. Rivas, J. Appl. Phycol. 5, 45(1993**)**.
[19] E. Gómez-Ordóñez, P. Rupérez, Food Hydrocolloids 25, 1514 (2011**)**.
[20] S. Brunauer, P.H. Emmett, E.Teller, J. Am. Chem. Soc. 60(2), 309 (1938).
[21] E.P. Barret, P.B. Joyner, P.Halenda, J. Am. Chem. Soc. 73, 373 (1951).
[22] C.S. Ciobanu, F. Massuyeau, E. Andronescu, M.S. Stan, A. Dinischiotu, D. Predoi, Dig. J. Nanomater. Bios. 6(4), 1639 (2011).
[23] S.L. Iconaru, M. Motelica-Heino, D. Predoi, Journal of spectroscopy, doi:10.1155/2013/284285 (2013)
[24] B.O. Fowler, Infrared studies of apatites. I. Inorg. Chem. 13, 194 (1974).
[25] A. Slosarczyk, Z. Paszkiewicz, C. Paluszkiewicz , J. Mol. Struct. 744–747, 657 (2005**)**.
[26] M. Lebon , I.Reiche , F.Fröhlich , J.-J.Bahain , C.Falguères, Anal. Bioanal. Chem. 392, 1479 (2008).
[27] M. Markovik, B.O. Fowler, M.S. Tung, J. Res. Natl. Inst. Stan. 109, 553 (2004).
[28] C. Castro Ribeiro, I. Gibson, M.A. Barbosa, Biomaterials 27, 1749 (2006).
[29] K. Nakamoto, (John Wiley and Sons, New York, 1978).
[30] R.Z. LeGeros, G. Bonel, R. Legros, Calcif. Tissue Res. 26, 111 (1978).
[31] D.W. Holcomb, R.A. Yung, Calcif. Tissue Int. 31, 189 (1980).
[32] J.C. Elliott, PhD Thesis, London University (London 1974).
[33] D.A. Lopez, S.R. de Sanchez, S.N. Simison, Electrochim. Acta. 48 (7), 845 (2003).
[34] J. Serra, P. Gonzalez, S. Liste, C .Serra, S. Chiussi, B. Leon, M. Perez-Amour, H.O. Ylanen, M. Hupa, J. Non-Cryst. Solids. 332, 20 (2003**)**.
[35] K. McLeod, S. Kumar, R St. Claire Smart, N.K. Dutta, N.H. Voelcker, G.I. Anderson, R. Sekel, Appl. Surf. Sci. 253, 2644 (2006**)**.

[36] M. Yoshinari , Y. Oda , H. Ueki , S. Biomaterials 22(7), 709 (2001**)**.
[37] J.F. Moulder, W.F. Stickle, P.E. Sobol, K.D. Bomben, Handbook of X-ray Photoelectron Spectroscopy, Physical Electronics Inc., Minnesota, USA, 1995.
[38] G. Gaggiotti, A. Galdikas, S. Kaciulis, G. Mattongo, A.Setkus, J. Appl. Phys. 76(8), 4467-(1994**)**.
[39] Takashi Kawabe, Satoshi Shimomura, Takashi Karasuda, Kenji Tabata, Eiji Suzuki, Yoichi Yamaguchi, Surf. Sci. 448, 101 (2000).
[40] M.S. Hegde, M. Ayyoob, Surf. Sci. 173(2-3), L635 (1986).
[41] C.N.R. Rao, V. Vijayakrishnan, G.U. Kulkarni, M.K. Rajumon, Appl. Surf. Sci. 84, 285 (1995**)**.
[42] G.U. Kulkarni, C.N.R. Rao, M.W. Roberts, Langmuir 11, 2572 (1995).
[43] S. Kaciulis, G. Mattogno, L. Pandolfi, M. Cavalli, G. Gnappi, A. Montenero, Appl. Surf. Sci. 151, 1 (1999).
[44] A. Boyd, M. Akay, B.J. Meenan, Surf. Interface Anal. 35, 188 (2003).
[45] T.F. Stoica, C. Morosanu, A. Slav, T. Stoica, P. Osiceanu, C. Anastasescu, M. Gartner, M. Zaharescu, Thin Solid Films 516, 8112 (2008).
[46] C. Battistoni, M.P Casaletto, G.M. Ingo, S. Kaciulis, G. Mattogno, L. Pandolfi, Surf. Interface Anal. 29(11), 773 (2000).
[47] A.J. Nathanael, D. Mangalaraj, S.I. Hong, Y. Masuda, Mater. Charact. 62, 1109(2011).
[48] K.S.W. Sing, D.H. Everett, R.A.W. Haul, L. Moscou, R.A. Pierotti, J. Rouquerol, T. Siemieniewska, Pure Appl. Chem. 57, 603 (1985**)**.
[49] Cuimiao Zhang, Chuncxia Li, Shanshan Huang, Zhiyao Hou, Ziyong Cheng, Piaoping Yang, Biomaterials 31, 3374 (2010).
[50] S.J. Gregg, K.S.W. Sing, (Academic Press, London, 1982).
[51] Y. Liu, C.Y. Liu, J.H. Wei, R. Xiong, C.X. Pan, J. Shi, Appl. Surf. Sci. 256, 6390 (2010).
[52] J. Leiser, B.A. Molitoris, Biochim. Biophys. Acta 1225, 1 (1993**)**.
[53] D.A. Parsell, S. Lindquist, Annu. Rev. Genet. 27, 437 (1993**)**.
[54] T.J. Webster, E.A. Massa-Schlueter, J.L. Smith, E.B. Slamovich, Biomaterials 25, 2111 (2004).
[55] M. Kheradmandfard, M.H. Fathi, J. Alloys. Compd. 504, 141 (2010**)**.
[56] A. Bianco, I. Cacciotti, M. Lombardi, L. Montanaro, E. Bemporad, M. Sebastiani, Ceram. Int. 36, 313 (2010).
[57] R.Z. Le Geros, G. Quirolgico, J.P. Le Geros, J. Dent. Res. 60B, 452 **(**1981).
[58] J. Christoffersen, M.R. Christoffersen, N. Kolthoff, O. Barenholdt, Bone 20, 47 (1997).
[59] C. Ergun, T.J. Webster, R. Bizios, R.H. Doremus, J. Biomed. Mater. Res. 59, 305 (2002).
[60] G. Bonel, G. Montel, Compt. Rend. 258, 923 (1964).
[61] R.Z. Le Geros, O.R. Trautz, J.P. Le Geros, E. Klein, Extrait du bulletin de la Societe´ Chimique de France, special number **(**1968)1712–1718.
[62] C. Yang, P.P. Yang, W.X. Wang, J. Wang, M.L. Zhang, J. Lin, J. Colloid Interf. Sci. 328, 203 (2008).
[63] Z.Y. Hou, P.P. Yang, H.Z. Lian, L.L. Wang, C.M. Zhang, C.X. Li, R.T. Chai, Z.Y. Cheng, J. Lin, Chem. Eur. J. 15, 6973 (2009).
[64] I.R. Gibson, S.M. Best, W. Bonfield, J. Biomed. Mater. Res. 44, 422 (1999).
[65] H. Owada, K. Yamashita, T. Umegaki, T. Kanazawa, M . Nagai, Solid State Ionics 35(3-4), 401(1989).
[66] P. Dancker, I. Low, W. Hasselbach, T. Wieland, Biochim. Biophys. Acta. 400, 407 (1975).

[67] Z. Spoerl, M. Stumpf, A.A. Noegel, A. Hasse, Oligomerization, J. Biol. Chem. 277(50), 48858 (2002).
[68] K.J. Kelly, Contrib. Nephrol. 148, 86 (2005).
[69] S.D. Westerheide, R.I. Morimoto, J. Biol. Chem. 280(39,) 33097 (2005).
[70] F. Amorim, P.L. Moseley (Springer Science Business Media B.V., Pedersen B.K., 2010)
[71] S.C. Gupta, A. Sharma, M. Mishra, R.K. Mishra, D.K. Chowdhuri Life Sci. 86, 377 (2010).
[72] B.M. Sanders, L.S. Martin, Sci. Total Environ. 139-140, 459 (1993).
[73] S.W.Y. Wong, P.T.Y. Leung, A.B. Djurišić, K.M.Y. Leung, Anal. Bioanal. Chem. 396, 609 (2010).
[74] M. Ahamed, R. Posqai, T.J. Gorey, M. Nielsen, S.M. Hussain, J.J. Rowe, Toxicol. Appl. Pharmacol. 242(3), 263 (2010).
[75] W.J. Chirico, M.G. Waters, G. Blobel, Nature 332, 805 (1988).
[76] S.M. Van der Vies, A.A. Gatenby, P.V. Vitanen, G.H. Lorimer, (American Chemical Society, Washington DC, 1993).
[77] K. Jimbow, Y. Tamura, A. Yoneta, T. Kamiya, I . Ono, T .Yamashita, A. Ito, H. Honda, K.Wakamatsu, S. Ito, S. Nohara, E. Nakayama, T. Kobayashi, J. Biomat. Nanobiotechnol. 3, 140 (2012).
[78] J. Xu, P. Xu, Z. Li, J. Huang, Z.Yang, J. Biomed. Mater. Res. A 100(3), 738 (2012).
[79] Z. Xu, C. Liu, J. Wei, J. Sun, J. Appl. Toxicol. 32(6), 429 (2012).